Journal of Peptide Science
J. Pept. Sci. 2008; **14**: 1129–1138
Published online 10 July 2008 in Wiley InterScience (www.interscience.wiley.com). DOI: 10.1002/psc.1050

JOURNAL OF PEPTIDE SCIENCE

The structure of S100A11 fragment explains a local structural change induced by phosphorylation‡

TAKAHIDE KOUNO,[a] MINEYUKI MIZUGUCHI,[a]* MASAKIYO SAKAGUCHI,[b] EIICHI MAKINO,[b] YOSHIHIRO MORI,[a] HIROYUKI SHINODA,[a] TOMOYASU AIZAWA,[c] MAKOTO DEMURA,[c] NAM-HO HUH[b] and KEIICHI KAWANO[c]

[a] Faculty of Pharmaceutical Sciences, University of Toyama, Toyama 930-0194, Japan
[b] Department of Cell Biology, Okayama University Graduate School of Medicine, Dentistry, and Pharmaceutical Sciences, Okayama 700-8558, Japan
[c] Division of Biological Sciences, Graduate School of Science, Hokkaido University, Sapporo 060-0810, Japan

Received 20 April 2008; *Revised 30 April 2008*; *Accepted 7 May 2008*

Abstract: S100A11 protein is a member of the S100 family containing two EF-hand motifs. It undergoes phophorylation on residue T10 after cell stimulation such as an increase in Ca^{2+} concentration. Phosphorylated S100A11 can be recognized by its target protein, nucleolin. Although S100A11 is initially expressed in the cytoplasm, it is transported to the nucleus by the action of nucleolin. In the nucleus, S100A11 suppresses the growth of keratinocytes through $p21^{CIP1/WAF1}$ activation and induces cell differentiation. Interestingly, the *N*-terminal fragment of S100A11 has the same activity as the full-length protein; i.e. it is phosphorylated *in vivo* and binds to nucleolin. In addition, this fragment leads to the arrest of cultured keratinocyte growth. We examined the solution structure of this fragment peptide and explored its structural properties before and after phosphorylation. In a trifluoroethanol solution, the peptide adopts the α-helical structure just as the corresponding region of the full-length S100A11. Phosphorylation induces a disruption of the N-capping conformation of the α-helix, and has a tendency to perturb its surrounding structure. Therefore, the phosphorylated threonine lies in the *N*-terminal edge of the α-helix. This local structural change can reasonably explain why the phosphorylation of a residue that is initially buried in the interior of protein allows it to be recognized by the binding partner. Copyright © 2008 European Peptide Society and John Wiley & Sons, Ltd.

Keywords: keratinocyte; MAK19 peptide; phosphorylation; S100A11; solution structure; trifluoroethanol

INTRODUCTION

S100 proteins have molecular weights of approximately 10 kDa and similar amino acid sequences with two EF-hand motifs [1,2]. To date, at least 25 proteins have been identified as members of the S100 family, and they usually exist as a homo- and heterodimers in specific cell types. Calcium binding to their EF-hands induces a conformational change, which triggers an interaction with target proteins [3,4]. S100 proteins are involved in a variety of physiological processes, such as regulation of cell growth, differentiation, motility and so on [1].

A member of the S100 protein family, S100A11 (also referred to as S100C and calgizarrin), was initially identified in porcine cardiac muscle and chicken gizzard smooth muscle [5,6]. It is predominantly present in the cytoplasm of human fibroblasts and keratinocytes, and colocalizes with actin filaments [7,8]. Interestingly, cell stimulation, such as an increase in Ca^{2+} concentration, changes the intracellular distribution of S100A11, leading to two distinct localizations: accumulation at the cell periphery and in the nuclei [9–11]. The former translocation relies on microtubule formation and results in the peripheral colocalization of S100A11 with annexin I, to which it binds, and is involved in membrane transport processes [7,12–15]. This complex participates in the formation of cornified envelopes, the process of terminal keratinocyte differentiation in the skin [16,17].

We previously studied in detail the second localization of S100A11 to the nucleus [11,18,19]. In keratinocytes stimulated by transforming growth factor beta1 (TGFβ1) or by an increase in Ca^{2+} levels, the cytosolic S100A11 is phosphorylated on residue T10 by the action of protein kinase Cα (PKCα), which enables S100A11 to bind to nucleolin. Nucleolin mediates signaling from the cell surface to the nucleus [20], and thereby nucleolin-bound S100A11 is transported into the nucleus. In the nucleus, S100A11 prompts Sp1 protein to dissociate from nucleolin, and the released Sp1 binds to the promoter region of $p21^{CIP1/WAF1}$ and activates its expression, cooperatively with Smad3 or NFAT1, which are introduced by distinct pathways originating from TGFβ1 receptor and calcineurin, respectively. It has been shown that $p21^{CIP1/WAF1}$ protein induces inhibition of Cdk activity and blockage of cell cycle progression [21].

Taken together, S100A11 acts to facilitate the differentiation and the cornification of keratinocytes both in cell nuclei and on the periphery. Consistent with

*Correspondence to: Mineyuki Mizuguchi, Faculty of Pharmaceutical Sciences, University of Toyama, Toyama 930-0194, Japan;
e-mail: mineyuki@pha.u-toyama.ac.jp

‡The ^{1}H chemical shifts and the atomic coordinates of MAK19 and pMAK19 have been deposited in the BioMagResBank as entries 6017 and 6018 and in the Protein Data Bank as entries 1V4Z and 1V50, respectively.

this, we previously observed that S100A11 is not found in the nuclei of the basal layer in which keratinocytes proliferate, but it can be detected in the nuclei of the suprabasal layers of skin [11].

Surprisingly, a peptide comprising the *N*-terminal 19 amino acid residues of S100A11 (termed as MAK19) acts as an intact protein with the same activity as the full-length sequence; i.e. it shows cytotoxicity and suppression of cell growth [22]. Another study showed that a fragment peptide (M1 to K23 of S100A11) undergoes phosphorylation on residue T10 in normal human cells, which leads to the interaction of the peptide with nucleolin [11]. Thus, MAK19 is able to mimic the actions of the full-length S100A11 *in vivo*.

Some groups have already reported the three-dimensional structures of full-length S100A11 as the apo-form and as a Ca^{2+}-binding complex with an annexin I fragment [4,23]. The S100A11 structure includes four α-helices (I–IV) and forms a homodimer through interactions between helices I/I′ and IV/IV′, which arrange individually in an antiparallel fashion. Residue C13 within helix I contacts C13′ of another monomer, and they are in a favorable position to form an intermolecular disulfide bridge without conformational changes [23]. Indeed, S100A11 dimer cross-linked by a disulfide bond has been found under nonreducing conditions [6]. In addition, the phosphorylation site T10 is located in the *N*-terminal region of helix I and is completely buried in the interior [4,23]. MAK19 peptide corresponds to the *N*-terminal half of helix I and the disordered region leading into helix I in the S100A11 structure. We investigated the solution structure of MAK19 and its phosphorylated form (pMAK19) by CD and NMR spectroscopy. Here we describe the structural properties of the functional peptide MAK19 and suggest a physiological significance for the structural change induced by phosphorylation of S100A11.

MATERIALS AND METHODS

Peptides

The peptides MAK19 (M-A-K-I-S-S-P-T-E-T-E-R-C-I-E-S-L-I-A), MAK19 phosphorylated on residue T10 (pMAK19) and pMAK19 homodimer were synthesized by Toray Research Center (Tokyo, Japan). MAK19 dimer was prepared according to the dimerization procedure described below. The purity and integrity of the peptides were confirmed by RP-HPLC and matrix-assisted laser desorption time-of-flight mass spectrometry. Peptide solution concentrations were measured by the method of Lowry [24] using reagents purchased from Bio-Rad Laboratories (Hercules, CA) and a protein standard, chicken egg albumin, purchased from Wako Pure Chemical Industries (Osaka, Japan).

Dimerization of MAK19 and pMAK19

Peptides MAK19 and pMAK19 were dissolved in 20 mM sodium phosphate buffer (pH 7.0) at a final concentration of approximately 1.0 mM. The peptide solutions were incubated at 25 °C. After incubation for 1, 2, 3 and 7 days, 10 µl aliquots were analyzed by RP-HPLC using a Wakosil 5C18 column (ϕ 4.0 mm × 250 mm). The components were eluted with a linear gradient of acetonitrile (20–35%) for 15 min in 0.05% trifluoroacetic acid, and detected by absorbance at 214 nm.

Circular Dichroism Spectroscopy

All CD spectra were recorded on a Jasco J-805 spectropolarimeter at 20 °C using a 1.0 mm quartz cell. Each peptide was dissolved in 20 mM sodium phosphate buffer (pH 7.0) to a final concentration of 0.1 mM. For titration experiments, the samples contained 0–60% TFE. To the solution of MAK19 and pMAK19 monomers 1 mM dithiothreitol was added. CD spectra of the monomers were not affected by the presence or absence of dithiothreitol. Spectra of all samples were corrected by using reference samples of similarly prepared solutions but in the absence of the peptide. Ellipticity was reported as mean residue molar ellipticity.

Nuclear Magnetic Resonance Spectroscopy

Each peptide was dissolved to a final concentration of approximately 2.0 mM in 250 µl of sample buffer, 20 mM sodium phosphate, pH 7.0, and 50% deuterated TFE (TFE-d_3)/50% H_2O, or 50% TFE-d_3/50% D_2O. To the solutions of MAK19 and pMAK19 monomers 5 mM deuterated dithiothreitol was added. Prior to the NMR experiments, the sample solutions were centrifuged at 15 000 *g* for 1 min to remove aggregated peptides. All NMR spectra were acquired at 293 K on a Bruker DMX500 spectrometer. DQF-COSY [25], two-dimensional TOCSY (mixing time 76 ms) [26] and NOESY (50, 100, 120, 150, and 200 ms) [27] spectra were acquired, with 4096 × 512 data points for DQF-COSY and 2048 × 512 data points for the other spectra. ^{1}H chemical shifts were directly referenced to the resonance of 2,2-dimethyl-2-silapentane-5-sulfonate sodium salt. The assignment of ^{1}H resonances of the backbone and side chains was performed using a series of two-dimensional NMR experiments as described previously [28]. ^{1}H resonance assignments of all MAK19 and pMAK19 peptides were achieved except for the residues M1 and A2. All NMR spectra were processed and analyzed using NMRPipe [29] and PIPP [30] software.

Structure Calculations

For structure calculations of MAK19 and pMAK19 peptides, distance restraints were collected from two-dimensional homonuclear NOESY spectra acquired with a 120 ms mixing time. The assignment of NOE cross-peaks was performed using a manual procedure. Interproton distance (r) was derived from the NOE intensity (S) with a relationship $r = c(S)^{1/6}$ in which c is a coefficient determined on the basis of NOE corresponding to a known distance: for the NOESY spectra in 50% TFE-d_3/50% H_2O solution, $H^N(i)$–$H^\alpha(i-1) = 1.70$–3.60 Å and $H^N(i)$–$H^\alpha(i) = 2.70$–3.05 Å for residues in the α-helix; for the NOESY spectra in 50% TFE-d_3/50% D_2O solution, H^α—$H^\beta = 2.50$–2.70 Å for alanine. A 50% error on the peak intensities was assumed, and the estimated interproton distance was used as an upper bound. For all interproton restraints, the lower bound was set to 1.80 Å. The calculation of MAK19 and

DOI: 10.1002/psc

pMAK19 dimers used disulfide bond information between C13 and C13′ as the distance restraints; specifically, the restraints for C13 S^{γ}—C13′ S^{γ} and C13 S^{γ}—C13′ C^{β} distances were assigned to be 2.00–2.10 and 3.00–3.10 Å, respectively. The $^{3}J_{HNH\alpha}$ coupling constant was derived from the DQF-COSY spectrum, and the dihedral angle (ϕ) restraints were set to $-65 \pm 25^{\circ}$ for residues with the $^{3}J_{HNH\alpha}$ value smaller than 9.0 Hz; although this criterion seems to be much larger than the general value, it is reasonable to identify a secondary structure in the case of MAK19 peptides with relatively large $^{3}J_{HNH\alpha}$ values. The NOE-derived distance and the dihedral angle restraints were used to calculate structures of MAK19 and pMAK19 peptides in X-PLOR using simulated annealing protocols [31]. A simulated annealing protocol was applied using 6000 steps at high temperature (1000 K) and 4000 steps for the cooling process. A total of 50 structures were calculated, and the 25 lowest-energy structures were used for calculation of the energy-minimized average structure. The obtained structures were analyzed with MOLMOL [32] and PROCHECK-NMR [33] software. Structural figures were generated using the MOLMOL program.

RESULTS

Self-dimerization of MAK19 and pMAK19

S100A11 can form a disulfide bond through the cysteine residue 13, leading to the formation of a homodimer [6,23]. The MAK19 peptide includes the corresponding cysteine residue. We examined the ability of MAK19 peptide to dimerize with a disulfide bond. Under nonreducing conditions, MAK19 and pMAK19 were incubated for one week. HPLC and mass spectrometry analyses indicated that MAK19 produces its homodimer, and more than half of MAK19 is present as a homodimer after one week (Figure 1).

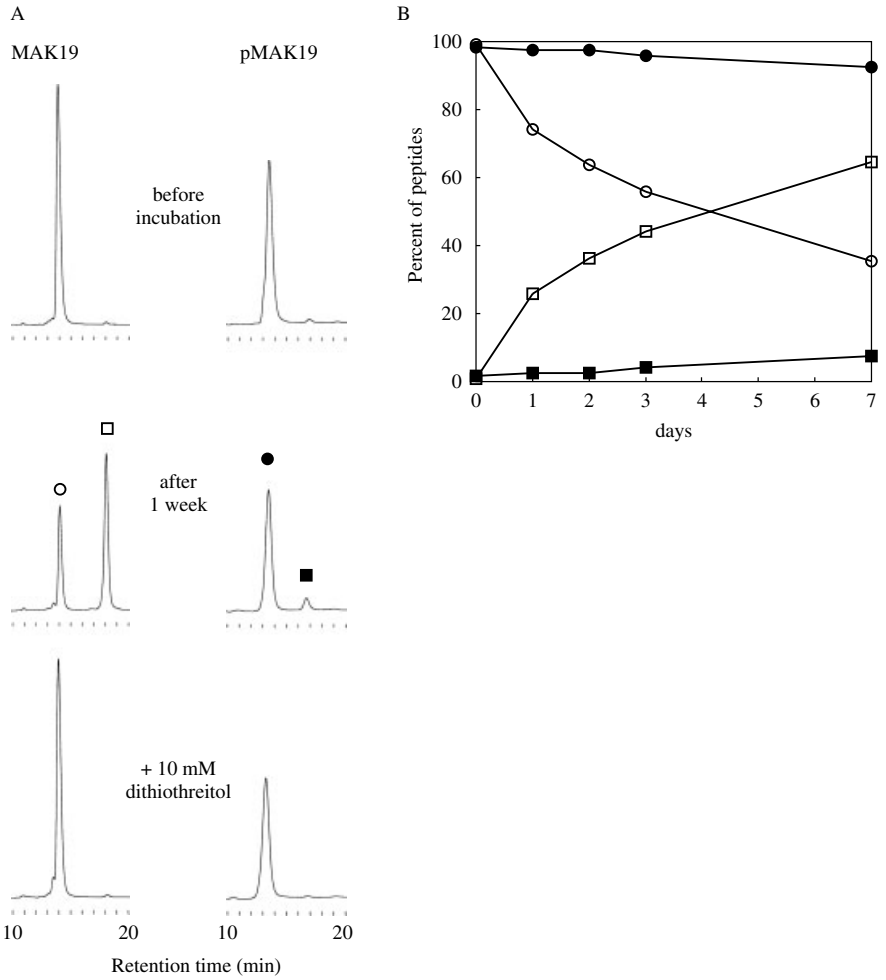

Figure 1 Dimerization Assay using MAK19 and pMAK19 peptides. MAK19 and pMAK19 were incubated without reducing agents. (A) Reverse-phase HPLC profiles before and after incubation indicated with an arbitrary scale of absorbance at 214 nm. Although both peptides initially showed a single peak (upper panel), a new peak corresponding to the dimer emerged after the incubation (middle panel). The addition of dithiothreitol (10 mM) into the incubated solution represents a single peak (lower panel). (B) The relative amount of each eluted component quantified with its peak area, and traced during the incubation. MAK19 monomer, MAK19 dimer, pMAK19 monomer and pMAK19 dimer are denoted by open circle, open rectangle, filled circle, and filled rectangle, respectively.

DOI: 10.1002/psc

In contrast, pMAK19 produced a small amount of homodimer. The addition of a reducing agent to each incubated solution yielded a single peak corresponding to the monomer, suggesting that both MAK19 and pMAK19 homodimers are supported by the disulfide bond. The results indicate that phosphorylation of T10 appreciably suppresses the formation of homodimers linked by disulfide bonds through C13.

CD Experiments

The CD spectrum of MAK19 monomer in aqueous solution was characterized by a negative peak at 200 nm (Figure 2(A)), suggesting that MAK19 monomer is primarily unstructured. As TFE was added to the solution, the shape of spectrum was gradually shifted up to 40–50% TFE. Further addition of TFE induced only a small change in the spectrum. Compared with the CD spectrum in the aqueous solution, the spectrum in 50% TFE has a larger minimum at 205 nm. In addition, the ellipticity remarkably decreased in the range 205–240 nm, while the opposite change was found at wavelengths below 205 nm, implying the formation of an α-helix in TFE solution. Notably, an explicit isodichroic point at 205 nm is indicative of an equilibrium between two conformational states; i.e. unstructured and α-helical conformations.

As with the MAK19 monomer, the conformation of disulfide-bonded homodimer of MAK19 changed depending on the concentration of TFE and showed an isodichroic point at 205 nm. In addition, the ellipticity at wavelengths above 205 nm was smaller than that of the MAK19 monomer in 50% TFE (Figure 2(B)). In general, the structural feature can be obtained from the ratio of the intensities of the minimum near 222 nm and another minimum between 200 and 210 nm; the ratio is close to zero for a random structure, while it approaches 1 in a highly helical state. In 50% TFE solution, the ratio for MAK19 monomer and dimer is 0.71 and 0.87, respectively. These differences in ellipticity are due to structural and/or population changes, such as an increase in helical conformation. MAK19 homodimer is also in equilibrium between random and α-helical conformations, and has a greater preference for the helical conformation than the MAK19 monomer.

The CD spectra of the pMAK19 monomer and dimer have essentially identical shapes and TFE dependence, like MAK19 peptides (data not shown). Therefore, TFE also prompts pMAK19 peptides to form an α-helix, and this action is enhanced in the homodimer of pMAK19. In other words, the CD experiments did not distinguish between MAK19 and pMAK19.

NMR Experiments

Consistent with the CD experiments, the inter-residual NOEs, including $d_{NN}(i, i+1)$ connectivities, were barely detectable on the NOESY spectrum of MAK19 in the aqueous solution (Figure 3(A)). This finding explicitly shows that MAK19 does not adopt any defined structure in the aqueous solution. In the presence of 50% TFE, many cross-peaks emerged on the NOESY spectrum, and the $d_{NN}(i, i+1)$ connectivity was found for residues expanding from T8 to I18 (Figure 3(B)). These consecutive $d_{NN}(i, i+1)$ connectivities constitute one of a number of typical patterns characterizing the formation of an α-helix. In addition to $d_{NN}(i, i+1)$, other connectivities that are diagnostic of α-helix formation, such as $d_{N\alpha}(i, i+3)$ and $d_{\alpha\beta}(i, i+3)$, are summarized in Figure 4. These patterns indicate that residues P7–I18 of the MAK19 monomer adopt the α-helical conformation in 50% TFE solution. Interestingly, this tendency is more evident in the disulfide-bonded homodimer of MAK19 (Figure 4(B)).

Like MAK19, pMAK19 also showed similar NOE connectivities indicative of α-helix formation (Figure 4(C)

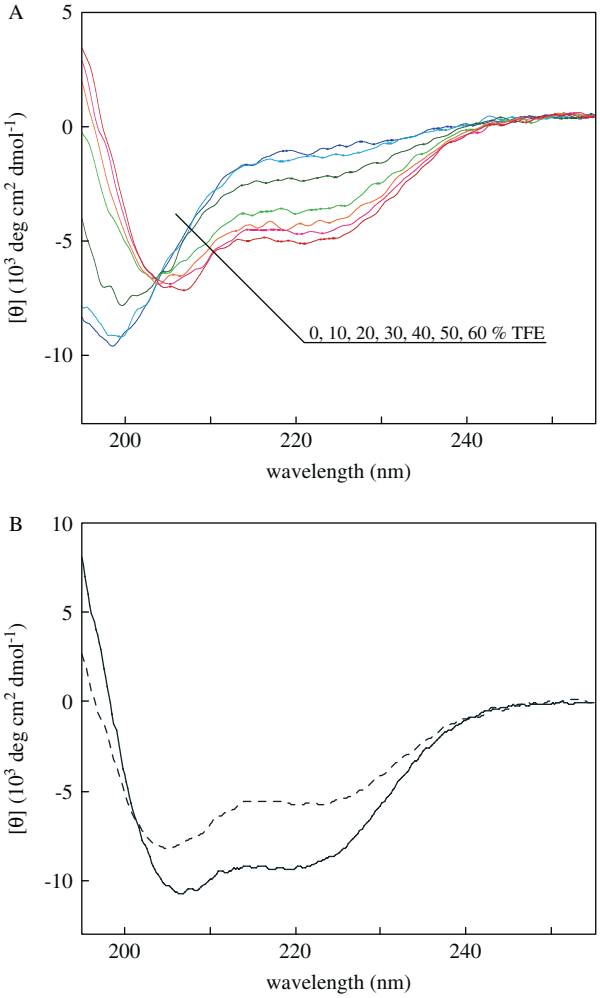

Figure 2 Far-ultraviolet CD spectra of MAK19 monomer and dimer. (A) CD spectra of MAK19 monomer recorded in various concentrations of TFE at 20 °C. The spectrum at each titration point is shown as a gradual shift from blue (0% TFE) to red (60% TFE). (B) CD spectra of MAK19 monomer (broken line) and its dimer (solid line) in 50% TFE solution.

DOI: 10.1002/psc

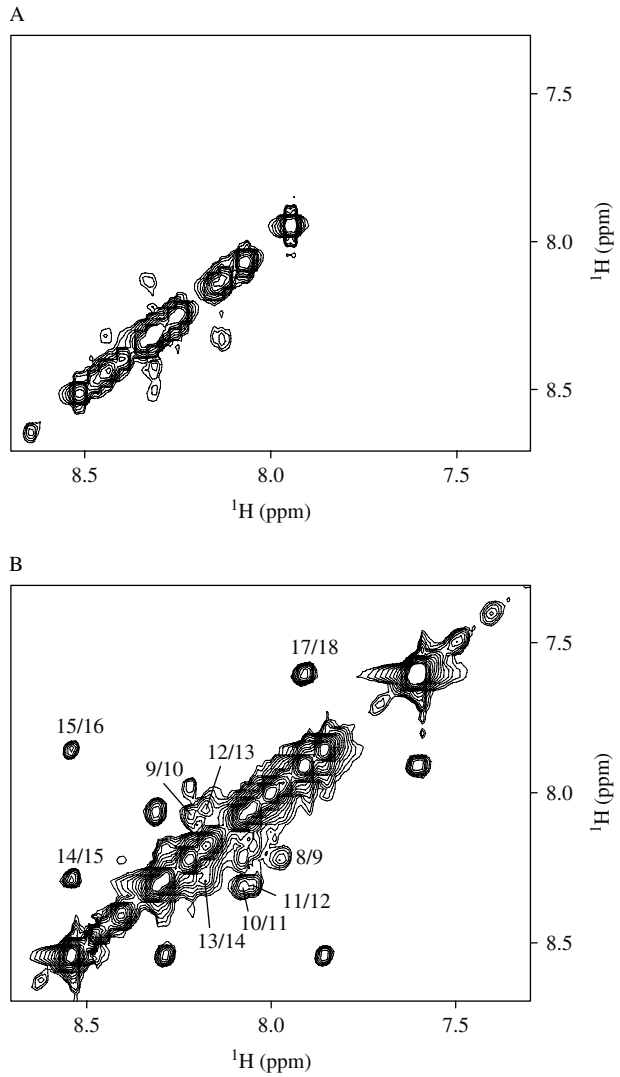

Figure 3 HN–HN region of NOESY spectra for MAK19. (A) In aqueous solution, MAK19 barely gave any cross-peaks in the region. (B) Some cross-peaks were observed in 50% TFE solution. Resonance assignments are indicated by residue numbers.

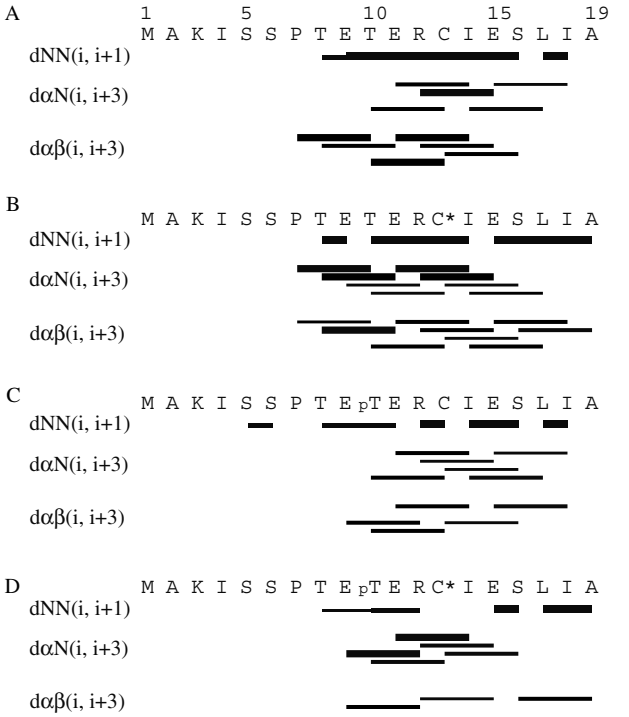

Figure 4 Summary of NOE connectivities that are characteristic of an α-helix structure. For each peptide, MAK19 monomer (A), MAK19 dimer (B), pMAK19 monomer (C) and pMAK19 dimer (D), NOESY spectra were acquired with 120 ms mixing time in 50% TFE solution. The thickness of lines represents the relative intensity of the corresponding NOE cross-peak, with thick lines indicating relatively strong peaks. In the amino acid sequence, pT and C* denote phosphorylated threonine and a half-cystine, respectively.

and (D)). However, in terms of $d_{N\alpha}(i, i+3)$ and $d_{\alpha\beta}(i, i+3)$, no NOE connectivity was found for P7 and T8 of both the pMAK19 monomer and dimer; this is not due to artifacts, such as a signal overlapping, or assignment ambiguity. Therefore, the α-helix of pMAK19 peptides was expected to expand from E9 to I18 (or from E9 to A19).

These differences between MAK19 and pMAK19 were visualized more explicitly by structure calculations using NMR-based restraints. The solution structures of four constructs, MAK19 monomer, MAK19 dimer, pMAK19 monomer and pMAK19 dimer, are shown in Figure 5, and the structural statistics are summarized in Table 1. They depict a bundle of 25 conformers with the lowest energy and the energy-minimized average structures for residues K3–A19 of each construct. Residues M1 and A2 were omitted because they did not give any signals on the NMR spectra. All four peptides commonly have a well-defined α-helix in the *C*-terminal half of the molecule, and the remaining region K3–S6 is disordered (Figures 5 and 6). The α-helix region in the average structure is P7–L17, P7–I18, E9–L17 and pT10–I18 for MAK19 monomer, MAK19 dimer, pMAK19 monomer and pMAK19 dimer, respectively. As described above, the difference was found in the conformation of residues P7 and T8. In the unphosphorylated forms of the MAK19 monomer and dimer, these residues are included in the α-helix with some degree of local convergence (Figure 6). In contrast, P7 and T8 of the pMAK19 monomer and dimer are no longer members of the α-helix and show a low degree of local convergence as with those of residues K3–S6. Moreover, residues E9 and pT10, immediately downstream of T8, also have a tendency to decrease convergence in the phosphorylated forms.

In general, secondary shifts measured by the difference between observed H^{α} and random coil chemical shifts are used for estimating secondary structures [34]. The secondary shift plot of MAK19 peptides shows only a weak tendency of α-helix

DOI: 10.1002/psc

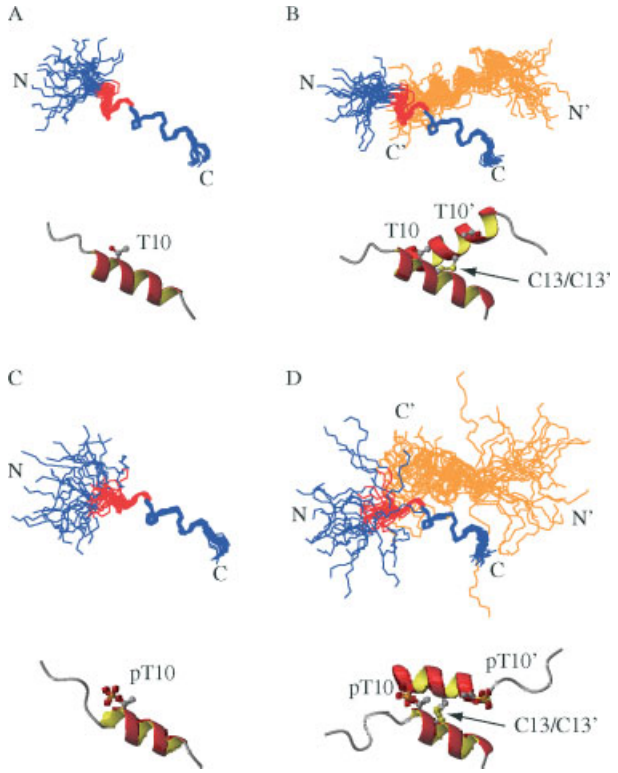

Figure 5 Solution structure of MAK19 peptides in 50% TFE solution. For each peptide, MAK19 monomer (A), MAK19 dimer (B), pMAK19 monomer (C) and pMAK19 dimer (D), a bundle of 25 conformers with the lowest energy and an energy-minimized average structure are shown. The backbone trace was always superimposed using the backbone heavy atoms (N, C^{α} and C′) for residues from T10 (pT10) to L17. In the dimer structure, the superimposition was performed for only one monomer, and another monomer is colored in orange. The backbone trace highlighted in red indicates a portion of residues P7–E9.

formation in the range from T10 (pT10) to E15 (Figure 7). Interestingly, the shift values in two regions, K3–S6 and E15–A19, are consistent for all four peptides. This implies that their local structures are not affected by phosphorylation on T10, nor by dimerization with disulfide bond C13/C13′. This finding is in agreement with the solution structure except for residues I18 and A19, which appear to adopt somewhat different conformations between the monomer and the dimer (Figure 5). On the other hand, the central region of the molecules, P7–I14, indicates a dispersion in the secondary shift values. In the *C*-terminal half of this region, E9–I14, the trace of the secondary shift value of the MAK19 monomer is accompanied by that of the pMAK19 monomer, and similarly for MAK19 and pMAK19 dimers. In addition, the H^{α} resonance of both dimers always emerged in the upfield side from that of the monomers except for residue C13. These features are likely to be due to dimerization, and agree with the results of CD experiments; i.e. α-helix formation is preferred in the dimer than in the monomer. Apart from this, a different pattern of the

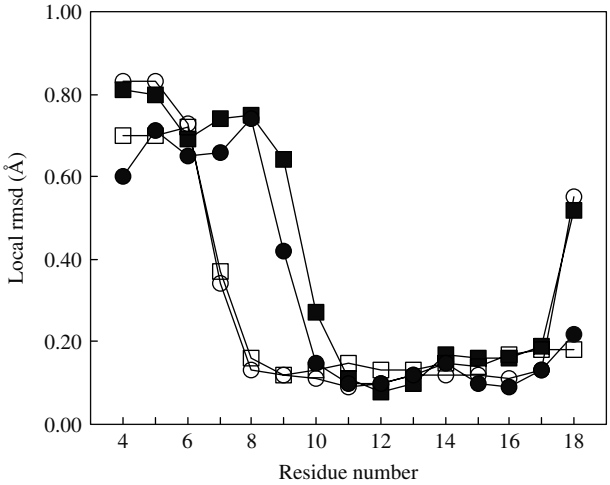

Figure 6 Local root mean-square deviation (rmsd) plot for backbone atoms. For each peptide, MAK19 monomer (open circle), MAK19 dimer (open rectangle), pMAK19 monomer (filled circle) and pMAK19 dimer (filled rectangle), three-residue average rmsds are plotted as a function of sequence.

secondary shift plot is found in residues P7 and T8. For these two residues, the secondary shift values of the pMAK19 monomer and dimer are almost identical, while those of the unphosphorylated MAK19 peptides show different values, and H^{α} resonance of the MAK19 dimer is shifted upfield more than that of the others. This upfield shift may indicate an enhancement of the helical conformation by dimerization, as in the case of residues E9–I14. Intriguingly, this effect does not appear for residues P7 and T8 of the phosphorylated forms (Figure 7).

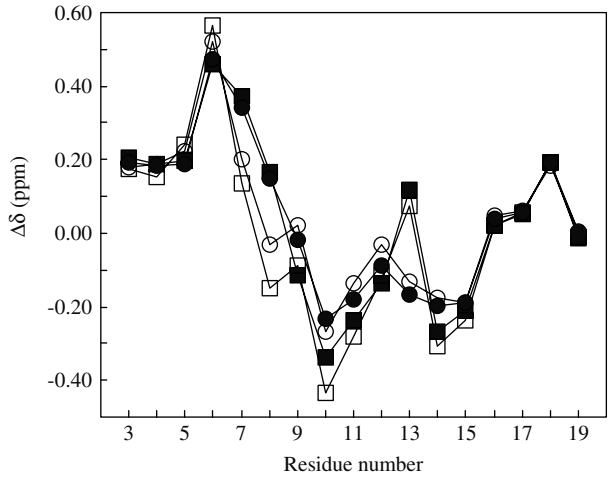

Figure 7 Secondary shift plot. For each peptide, MAK19 monomer (open circle), MAK19 dimer (open rectangle), pMAK19 monomer (filled circle) and pMAK19 dimer (filled rectangle), the H^{α} chemical shift values in 50% TFE solution were compared with random coil chemical shift values. Negative (upfield) $\Delta\delta$ values are associated with helical structure.

DOI: 10.1002/psc

Table 1 Structural statistics for the 25 lowest-energy structures of MAK19 peptides

	MAK19 monomer	MAK19 dimer	pMAK19 monomer	pMAK19 dimer
NOE-derived distance restraints[a]				
Intrachain	156	188	143	154
Interchain	—	5	—	3
Dihedral angle (ϕ) restraints[a]	11	7	6	0
X-PLOR energies (kJ mol^{-1})[b]				
E_{total}	22.03 ± 0.24	46.69 ± 0.82	24.51 ± 0.21	56.34 ± 0.92
E_{bonds}	0.47 ± 0.03	1.10 ± 0.09	0.56 ± 0.04	2.56 ± 0.16
E_{angles}	17.78 ± 0.12	36.11 ± 0.35	18.58 ± 0.12	37.77 ± 0.46
$E_{improper}$	2.96 ± 0.04	6.16 ± 0.07	3.01 ± 0.03	6.13 ± 0.15
$E_{van\ der\ Waals}$	0.07 ± 0.05	0.44 ± 0.28	0.85 ± 0.15	0.68 ± 0.33
E_{NOE}	0.75 ± 0.20	2.87 ± 0.63	1.50 ± 0.22	9.20 ± 0.64
$E_{dihedral}$	0	0	0	—
Root mean-square deviation (rmsd) from idealized covalent geometry[b]				
Bonds (Å)	0.001327 ± 0.000047	0.001442 ± 0.000058	0.001448 ± 0.000045	0.002184 ± 0.000068
Angles (°)	0.4901 ± 0.0016	0.4939 ± 0.0024	0.4980 ± 0.0016	0.5020 ± 0.0031
Improper (°)	0.4040 ± 0.0026	0.4124 ± 0.0024	0.4061 ± 0.0023	0.4093 ± 0.0049
Ramachandran plot (%)[b]				
Most favored	84.1	80.6	88.2	75.8
Additional allowed	11.1	17.1	8.7	19.9
Generously allowed	3.1	2.3	2.4	2.3
Disallowed region	1.7	0.0	0.7	2.0
Pairwise atomic rmsd (Å)				
Residues included in α-helix	P7-L17	P7-I18	E9-L17	pT10-I18
Backbone heavy atoms	0.52 ± 0.16	0.57 ± 0.17	0.47 ± 0.16	0.50 ± 0.16
(For two α-helices in a dimer)	—	1.10 ± 0.32	—	1.62 ± 0.64
All heavy atoms	1.32 ± 0.21	1.37 ± 0.21	1.40 ± 0.25	1.24 ± 0.19
(For two α-helices in a dimer)	—	1.81 ± 0.30	—	2.50 ± 0.74

[a] In the dimer, the number of restraints were collected for each monomer.
[b] Because the dimer was treated as a tandem repeat of the monomer in the X-PLOR calculations, the values for the dimer structure were estimated over the whole molecule.

Comparing the solution structures of MAK19 and pMAK19 dimers, the overall structure of the pMAK19 dimer shows an apparently lower convergence than that of the MAK19 dimer (Figure 5 and Table 1). One helix forms an angle of $150 \pm 15^{\circ}$ with another helix in 25 conformers of the pMAK19 dimer, and the configuration of two α-helices linked by a disulfide bond appears to be considerably perturbed. In the 25 lowest-energy conformers of the MAK19 dimer, two α-helices make a more acute angle of $119 \pm 9^{\circ}$, and its global structure appears to be relatively determined. This reflects a difference of NOE-derived distance restraints used for the structure calculations. While the MAK19 dimer gave some apparent interchain NOEs, the pMAK19 dimer only yielded a smaller number of interchain NOEs with a relatively low intensity (Table 1). For example, in terms of an interchain cross-peak between C13 $H^{\beta 1,2}$ and L17′ $H^{\delta 1}$, which is separated completely from other signals, the normalized intensity in the pMAK19 dimer decreased by almost threefold compared to that of the MAK19 dimer. These findings imply a local structural change and/or a conformational inhomogeneity in the pMAK19 dimer.

DISCUSSION

Effect of the Phosphorylation on T10 of MAK19

The dimerization assay using MAK19 peptides showed that phosphorylation leads to a substantial decrease in the yield of pMAK19 dimer supported by a disulfide bond. In general, a thiolate anion of cysteine triggers the formation of a new disulfide bond, and its reaction rate is affected by the environment, such as pH, charges, steric hindrances, and so on [35]. In particular, negative charges near the thiol tend to destabilize the thiolate and decrease the reaction rate. In the case of the present study, the phosphorylated threonine residue is located proximal to C13, so that the charges of the phoshoryl group are most likely to decrease the population of the thiolate anions, thereby causing a smaller yield of pMAK19 dimers.

NMR analysis showed that MAK19 peptides form α-helical structures before and after phosphorylation in TFE solution. It has been generally suggested that the dielectric constant of TFE approximates that of the interior of protein, and TFE prompts intramolecular

DOI: 10.1002/psc

hydrogen bonds of a protein to strengthen, so that secondary structures are stabilized [36]. In the overall structure of S100A11, the residues included in the first α-helix (helix I) make contact with hydrophobic side chains of other portions of the protein [4,23]. In addition, helices I and I′ form an angle of $-137 \pm 3^{\circ}$ in the solution structure of the full-length S100A11 dimer; i.e. this represents a mirror image of the structure of the MAK19 dimer. However, both share the residues participating in an interface between the helices; residues T10, C13 and L17 of MAK19 make contacts with another helix, like the full-length S100A11. Considering that the MAK19 peptide has an amino acid sequence corresponding to the *N*-terminal half of helix I and the disordered region leading into helix I of an intact S100A11, TFE is likely to reproduce appropriately the environment in which the MAK19 sequence originally is located.

The unphosphorylated MAK19 monomer and dimer form α-helices with *N*-terminal serine capping; i.e. S6, P7, and E9 are assigned to N-cap, N1, and N3, respectively, according to the nomenclature of Richardson and Richardson [37]. This is also supported by an NOE observation between the amide of S6 and the side chain of E9 as well as other peptides with serine capping [38]. Interestingly, this serine capping is not found in the structure of the pMAK19 monomer and dimer. This means that the length of the helix is shortened by phosphorylation, resulting in residue pT10 being located at the *N*-terminal edge of the helix. This local structural change may be due to steric hindrance and/or the electrostatic influence of the phosphoryl group attached to the side chain of T10. At first, in the structure of both the MAK19 monomer and dimer, the H^{α} atom of P7 is proximal to the H^{β} atom of T10, as supported by an observation of the NOE cross-peak between them (Figure 4). The presence of a bulky phosphoryl group would interfere with this contact, leading to the destruction of the α-helix. The α-helix is also known to have a dipole moment with a positive polarity at the *N*-terminal edge. It originates from a regular configuration of the backbone amide groups; i.e. the NH and CO groups are always aligned toward the *N*-terminus and *C*-terminus of the α-helix, respectively. This shows that the NH groups of residues T10 and E11 of MAK19 make hydrogen bonds with the CO groups of S6 and P7 as shown in its solution structure. Because a phosphoryl group has a negative charge, the phosphorylated T10 of pMAK19 is expected to easily disturb the contact of CO groups of S6 and P7 to HN groups of pT10 and E11. In addition, the steric and electrostatic features of pT10 would affect not only the intrachain structure but also the interchain configuration of the two α-helices of the pMAK19 dimer. This idea is also supported by the secondary shift value of P7 and T8 of MAK19 and pMAK19 dimers. MAK19 dimerization shows an upfield shift of H^{α} resonance of P7 and T8, implying that MAK19 dimerization stabilizes the α-helix and increases the population adopting the α-helical conformation. In contrast, the secondary shift value remains unchanged in pMAK19 dimerization. It is likely that the conformational change and stabilization do not occur in the pMAK19 dimer. Therefore, an apparent dispersion of the global structure of the pMAK19 dimer, compared with that of the MAK19 dimer, may reflect an essential inhomogeneity of the solution structure.

Physiological Significance of the Structural Change Induced by Phosphorylation

S100A11 undergoes phosphorylation on T10 by the action of PKCα *in vivo*, leading to an interaction with nucleolin [20]. However, this threonine residue is initially buried in the interior of the protein, as evidenced by NMR analysis using the full-length S100A11; i.e. the side chain of the residue corresponding to T10 of MAK19 generates NOE cross-peaks with residues located in other parts of the protein [4]. Our study shows that the *N*-terminal part of the α-helix in MAK19 is disrupted by phosphorylation on residue T10. This structural change means that phosphorylated threonine pT10 is exposed to the *N*-terminal edge of the α-helix. In addition, the phosphorylation has a tendency to perturb an arrangement of two α-helices in the MAK19 dimer. These features of MAK19 peptides allow us to conclude that phosphorylation of S100A11 induces a structural perturbation in the *N*-terminal edge of helix I, and enables the phosphoryl group to be exposed to the solvent. This suggestion can reasonably explain how phosphorylation on the initially buried residue is recognized by its binding partner nucleolin. Recently, it was shown that S100A11 is secreted from keratinocytes to the extracellular space, and then binds to RAGE, a receptor expressed in keratinocytes, resulting in an enhancement of cell growth [39]. Interestingly, S100A11 dimer linked by a disulfide bond facilitates the binding of S100A11 to RAGE. This finding gives a potential meaning to the observation that formation of MAK19 dimer through a disulfide bond is prevented by phosphorylation on T10. The phosphorylation of S100A11 may interfere with the binding of the secreted S100A11 to RAGE.

In general, it is difficult to explore the structural features of phosphorylated forms of large proteins because it is hard to prepare a large amount of a homogeneously phosphorylated target. An analysis using a peptide fragment derived from a large protein enables us to observe the effect of phosphorylation on the protein structure, as shown in this study. Moreover, the MAK19 peptide by itself acts as a full-length S100A11 *in vivo*, meaning that its phosphorylated form is recognized by nucleolin, and that it suppresses

DOI: 10.1002/psc

cell growth [11,22]. Further structural analysis using the MAK19 peptide, for example the determination of a complex structure between MAK19 and nucleolin, will shed light on why MAK19 can behave as an intact S100A11 protein, and at the same time help to explain the mechanism of S100A11 actions *in vivo*.

Acknowledgements

This study was supported by grants from the Ministry of Education, Culture, Sports, Science and Technology of Japan (MEXT) and by the National Project on Protein Structural and Functional Analyses (MEXT).

REFERENCES

1. Santamaria-Kisiel L, Rintala-Dempsey AC, Shaw GS. Calcium-dependent and -independent interactions of the S100 protein family. *Biochem. J.* 2006; **396**: 201–214.
2. Schaub MC, Heizmann CW. Calcium, troponin, calmodulin, S100 proteins: from myocardial basics to new therapeutic strategies. *Biochem. Biophys. Res. Commun.* 2008; **369**: 247–264.
3. Potts BC, Smith J, Akke M, Macke TJ, Okazaki K, Hidaka H, Case DA, Chazin WJ. The structure of calcyclin reveals a novel homodimeric fold for S100 Ca^{2+}-binding proteins. *Nat. Struct. Biol.* 1995; **2**: 790–796.
4. Dempsey AC, Walsh MP, Shaw GS. Unmasking the annexin I interaction from the structure of Apo-S100A11. *Structure* 2003; **11**: 887–897.
5. Ohta H, Sasaki T, Naka M, Hiraoka O, Miyamoto C, Furuichi Y, Tanaka T. Molecular cloning and expression of the cDNA coding for a new member of the S100 protein family from porcine cardiac muscle. *FEBS Lett.* 1991; **295**: 93–96.
6. Todoroki H, Kobayashi R, Watanabe M, Minami H, Hidaka H. Purification, characterization, and partial sequence analysis of a newly identified EF-hand type 13-kDa Ca^{2+}-binding protein from smooth muscle and non-muscle tissues. *J. Biol. Chem.* 1991; **266**: 18668–18673.
7. Naka M, Qing ZX, Sasaki T, Kise H, Tawara I, Hamaguchi S, Tanaka T. Purification and characterization of a novel calcium-binding protein, S100C, from porcine heart. *Biochim. Biophys. Acta* 1994; **1223**: 348–353.
8. Sakaguchi M, Miyazaki M, Inoue Y, Tsuji T, Kouchi H, Tanaka T, Yamada H, Namba M. Relationship between contact inhibition and intranuclear S100C of normal human fibroblasts. *J. Cell Biol.* 2000; **149**: 1193–1206.
9. Broome A-M, Eckert RL. Microtubule-dependent redistribution of a cytoplasmic cornified envelope precursor. *J. Invest. Dermatol.* 2003; **122**: 29–38.
10. Sakaguchi M, Miyazaki M, Kondo T, Namba M. Up-regulation of S100C in normal human fibroblasts in the process of aging in vitro. *Exp. Gerontol.* 2001; **36**: 1317–1325.
11. Sakaguchi M, Miyazaki M, Takaishi M, Sakaguchi Y, Makino E, Kataoka N, Yamada H, Namba M, Huh NH. S100C/A11 is a key mediator of Ca^{2+}-induced growth inhibition of human epidermal keratinocytes. *J. Cell Biol.* 2003; **163**: 825–835.
12. Meers P, Mealy N, Pavlotsky N, Tauber AI. Annexin I-mediated vesicular aggregation: mechanism and role in human neutrophils. *Biochemistry* 1992; **31**: 6372–6382.
13. Mailliard WS, Haigler HT, Schlaepfer DD. Calcium-dependent binding of S100C to the N-terminal domain of annexin I. *J. Biol. Chem.* 1996; **271**: 719–725.
14. Seemann J, Weber K, Gerke V. Structural requirements for annexin I-S100C complex-formation. *Biochem. J.* 1996; **319**: 123–129.
15. Davey GE, Murmann P, Hoechli M, Tanaka T, Heizmann CW. Calcium-dependent translocation of S100A11 requires tubulin filaments. *Biochim. Biophys. Acta* 2000; **1498**: 220–232.
16. Robinson NA, Lapic S, Welter JF, Eckert RL. S100A11, S100A10, annexin I, desmosomal proteins, small proline-rich proteins, plasminogen activator inhibitor-2, and involucrin are components of the cornified envelope of cultured human epidermal keratinocytes. *J. Biol. Chem.* 1997; **272**: 12035–12046.
17. Candi E, Schmidt R, Melino G. The cornified envelope: a model of cell death in the skin. *Nat. Rev. Mol. Cell Biol.* 2005; **6**: 328–340.
18. Sakaguchi M, Miyazaki M, Sonegawa H, Kashiwagi M, Ohba M, Kuroki T, Namba M, Huh NH. PKCα mediates TGFβ-induced growth inhibition of human keratinocytes via phosphorylation of S100C/A11. *J. Cell Biol.* 2004; **164**: 979–984.
19. Sakaguchi M, Sonegawa H, Nukui T, Sakaguchi Y, Miyazaki M, Namba M, Huh NH. Bifurcated converging pathways for high Ca^{2+}- and TGFβ-induced inhibition of growth of normal human keratinocytes. *Proc. Natl. Acad. Sci. U.S.A.* 2005; **102**: 13921–13926.
20. Shibata Y, Muramatsu T, Hirai M, Inui T, Kimura T, Saito H, McCormick LM, Bu G, Kadomatsu K. Nuclear targeting by the growth factor midkine. *Mol. Cell. Biol.* 2002; **22**: 6788–6796.
21. Missero C, Di Cunto F, Kiyokawa H, Koff A, Dotto GP. The absence of $p21^{Cip1/WAF1}$ alters keratinocyte growth and differentiation and promotes ras-tumor progression. *Genes Dev.* 1996; **10**: 3065–3075.
22. Makino E, Sakaguchi M, Iwatsuki K, Huh NH. Introduction of an N-terminal peptide of S100C/A11 into human cells induces apoptotic cell death. *J. Mol. Med.* 2004; **82**: 612–620.
23. Réty S, Osterloh D, Arié J-P, Tabaries S, Seeman J, Russo-Marie F, Gerke V, Lewit-Bentley A. Structural basis of the Ca^{2+}-dependent association between S100C (S100A11) and its target, the N-terminal part of annexin I. *Structure* 2000; **8**: 175–184.
24. Lowry OH, Rosebrough NJ, Farr AL, Randall RJ. Protein measurement with the Folin phenol reagent. *J. Biol. Chem.* 1951; **193**: 265–275.
25. Rance M, Sørensen OW, Bodenhausen G, Wagner G, Ernst RR, Wüthrich K. Improved spectral resolution in cosy ^{1}H NMR spectra of proteins via double quantum filtering. *Biochem. Biophys. Res. Commun.* 1983; **117**: 479–485.
26. Braunschweiler L, Ernst RR. Coherence transfer by isotropic mixing: application to proton correlation spectroscopy. *J. Magn. Reson.* 1983; **53**: 521–528.
27. Kumar A, Ernst RR, Wüthrich K. A two-dimensional nuclear Overhauser enhancement (2D NOE) experiment for the elucidation of complete proton-proton cross-relaxation networks in biological macromolecules. *Biochem. Biophys. Res. Commun.* 1980; **9**: 1–6.
28. Wüthrich K. *NMR of Proteins and Nucleic Acid*. John Wiley and Sons: New York, 1986.
29. Delaglio F, Grzesiek S, Vuister GW, Zhu G, Pfeifer J, Bax A. NMRPipe: a multidimensional spectral processing system based on UNIX pipes. *J. Biomol. NMR* 1995; **6**: 277–293.
30. Garrett DS, Powers R, Gronenborn AM, Clore GM. A common sense approach to peak picking two-, three- and four-dimensional spectra using automatic computer analysis of contour diagrams. *J. Magn. Reson.* 1991; **95**: 214–220.
31. Brünger AT. *X-PLOR Version 3.1*. Yale University Press: New Haven, CT, 1992.
32. Koradi R, Billeter M, Wüthrich K. MOLMOL: a program for display and analysis of macromolecular structures. *J. Mol. Graphics* 1996; **14**: 51–55.
33. Laskowski RA, Rullman JA, MacArthur MW, Kaptein R, Thornton JM. AQUA and PROCHECK-NMR: programs for checking the quality of protein structures solved by NMR. *J. Biomol. NMR* 1996; **8**: 477–486.

34. Wishart DS, Sykes BD, Richards FM. Relationship between nuclear magnetic resonance chemical shift and protein secondary structure. *J. Mol. Biol.* 1991; **222**: 311–333.
35. Torchinsky YM. *Sulfur in Proteins*. Pergamon Press: New York, 1981.
36. Nelson JW, Kallenbach NR. Stabilization of the ribonuclease S-peptide α-helix by trifluoroethanol. *Proteins* 1986; **1**: 211–217.
37. Richardson JS, Richardson DC. Amino acid preferences for specific locations at the ends of α helices. *Science* 1988; **240**: 1648–1652.
38. Lyu PC, Wemmer DE, Zhou HX, Pinker RJ, Kallenbach NR. Capping interactions in isolated α helices: position-dependent substitution effects and structure of a serine-capped peptide helix. *Biochemistry* 1993; **32**: 421–425.
39. Sakaguchi M, Sonegawa H, Murata H, Kitazoe M, Futami J, Kataoka K, Yamada H, Huh NH. S100A11, an dual mediator for growth regulation of human keratinocytes. *Mol. Biol. Cell* 2008; **19**: 78–85.

DOI: 10.1002/psc